Nonmonotonic Aging and Memory in a Frictional Interface

Sam Dillavou and Shmuel M. Rubinstein

Nonmonotonic Aging and Memory in a Frictional Interface

Sam Dillavou[1], Shmuel M. Rubinstein[2]

[1]*Physics, Harvard University, Cambridge, Massachusetts 02138, USA*
[2]*Applied Physics, Harvard University, Cambridge, Massachusetts 02138, USA*
(Dated: May 7, 2018)

We measure the static frictional resistance and the real area of contact between two solid blocks subjected to a normal load. We show that following a two-step change in the normal load the system exhibits nonmonotonic aging and memory effects, two hallmarks of glassy dynamics. These dynamics are strongly influenced by the discrete geometry of the frictional interface, characterized by the attachment and detachment of unique microcontacts. The results are in good agreement with a theoretical model we propose that incorporates this geometry into the framework recently used to describe Kovacs-like relaxation in glasses as well as thermal disordered systems. These results indicate that a frictional interface is a glassy system and strengthen the notion that nonmonotonic relaxation behavior is generic in such systems.

Under constant load, the static coefficient of friction of rock [1], paper [2], metal [3], and other materials [4, 5] grows logarithmically ad infinitum. This aging phenomenon is central to frictional systems ranging from micro-machines [6] to the earthquake cycle [7–9], and is described by the Rate and State Friction laws [10–12], where aging is captured by the evolution of a phenomenological state parameter. Because most solids have microscopically rough surfaces, when two bodies are brought together, their real area of contact is localized to an ensemble of microcontacts, which sets the frictional strength [13–16]. Thus, the strengthening of the interface is frequently attributed to a gradual increase of the real area of contact [4, 17]; however, recent compelling evidence suggests that such an effect could also result from the strengthening of interfacial bonds [18, 19].

Recently [20], it was shown that some systems which exhibit slow relaxation and logarithmic aging can also evolve non-monotonically under static conditions, exhibiting a memory effect, similar to the canonical memory effect discovered by Kovacs in polymers [21]. Several glassy and disordered systems ranging from polymer glasses [21] to crumpled paper [20] and granular piles [22] exhibit Kovacs-like non-monotonic relaxation. Previous observations of de-aging [23] in real area of contact suggest that unlubricated frictional interfaces may also belong to this universality class. If so, this may indicate that dynamics of friction exhibit a memory effect that is richer than previously considered; these dynamics cannot be fully captured by Rate and State with a single state parameter, or indeed any theory with a single degree of freedom.

Here we experimentally demonstrate that a dry frictional interface indeed exhibits a Kovacs-like memory effect. Using real time optical and mechanical measurements, we observe that under a constant load, both the static coefficient of friction and the real area of contact may evolve non-monotonically. Additionally, in contrast to the prevailing paradigm, the two physical quantities do not always evolve in tandem; in fact, one may grow while the other shrinks. We further show that this discrepancy arises from the non-uniform evolution of the contact surface. We propose a model that generalizes the geometrical descriptions of contact mechanics to include memory effects and the glassy nature of frictional interfaces.

Frictional dynamics are typically described through a force measurement, but understanding the underlying mechanisms requires observation of the 2D interface where shear forces are generated. We thus simultaneously measure the static friction coefficient and real area of contact resolved across an entire interface. Our biaxial compression and translation stage is described schematically in Fig. 1(a). The interface is formed between two laser-cut PMMA (poly methyl-methacrylate) blocks with 0.5 to 4 cm^2 of nominal contact area. Sample surface roughness ranges from the original extruded PMMA (11 nm RMS) to surfaces lapped with 220 grit polishing paper (1.8 μm RMS) [24]. A normal load, F_N, is applied to the top sample through a spring and load cell, and the bottom sample is held by a frame on a horizontal frictionless translation stage. A shear force, F_S, is applied to the bottom frame at the level of the interface by advancing a stiff load cell at a constant rate of 0.1 or 0.33 mm/s. We define the coefficient of static friction, μ_S as the peak shear force value prior to interfacial slip, divided by F_N. The effect of frictional memory is subtle, and observing it requires many runs, systematically varying multiple parameters. However, sliding wears the samples, which causes μ_S to vary systematically over the course of many measurements, as shown by the raw data (red) in Fig. 1(b). In order to differentiate the system's response to a change in the experimental parameters from its slow, background evolution due to wear, we implement a randomization protocol. We test all points of interest in our parameter space once in a random order, then again in a different random order, and so on, such that every point is visited a minimum of 25 times. Additionally, all cycles are normalized to have the same mean, as shown by the adjusted data (black) in Fig. 1(b). Fi-

nally, to minimize the uncertainty associated with initial placement and loading of the samples [25], we follow two pre-stress protocols [26], consistent with previous experiments [25, 27, 28]

The real area of contact between the blocks, A_R, is measured by using total internal reflection (TIR) [29, 30]. Blue light (473 nm) is incident on the top surface of the bottom sample at an angle below the critical angle for TIR, allowing light to escape into the top sample only through points of contact, as depicted in the bottom of Fig. 1(a). When imaged through the top sample, the brightness of the interface corresponds to real contacts, as shown in the inset in Fig. 1(c). When F_N is increased, microcontacts grow in size and number [17], which allows more light to pass through the interface; thus, the spatially integrated light intensity within the interface, $I(F_N)$, is a smooth, nonlinear, and monotonic function of the normal load, as shown in Fig. 1(d), consistent with previous observations [31]. The real area of contact evolves in time; however, for sufficiently rapid normal loading, in our case faster than 30N/s, the linear relationship $F_N = A_R\bar{\sigma}$ holds, where $\bar{\sigma}$ is the average contact pressure. This relationship holds for a wide variety of materials and contact models [13, 15–17, 31]. Thus, to convert the light intensity to the real area of contact, a conversion function $I = g(F_N) = g(A_R\bar{\sigma})$ is fit individually for each experiment. To avoid ambiguity, we only use $I(F_N)$ during the initial rapid loading. This calibration is used throughout the experiment to convert intensity to real area of contact: $g^{-1}(I(F_N,t))/\bar{\sigma} = A_R(F_N,t)$. As the magnitude of A_R does not effect our results, we may assume the fully plastic Bowden and Tabor picture [13], $\bar{\sigma} = \sigma_Y$, without loss of generality. Later we introduce a model that also considers elasto-plastic deformation.

We test for memory using a two-step protocol, previously used for other mechanical systems [20], as shown for a typical example in Fig. 2(a). The blocks are rapidly loaded from above to $F_N = F_1$ and are held constant at that load for a time T_W. During this first step, the real area of contact grows logarithmically in time:

$$\Delta A_R(t) = \beta_1 \log(t) \qquad (1)$$

consistent with previous observations [17, 23]. At $t = T_W$, the normal load is rapidly reduced to $F_N = F_2$ and kept constant for the remainder of the experiment. As a result of the reduction in normal load, many microcontacts instantly detach, showing a simultaneous drop in A_R, as shown at $t = 1000$s in Fig. 2(a). We refer to this instantaneous drop as the elastic response, distinct from the subsequent slow aging. For $t > T_W$, the evolution of A_R is non-monotonic, as shown in Fig. 2(b). Initially, the real area of contact shrinks in time. This de-aging effect [23], or weakening, may persist for seconds, minutes, or even hours until A_R reaches a minimum at time, T_{min}^A. After this time, A_R increases monotonically, eventually recovering typical logarithmic aging. This is a nontrivial
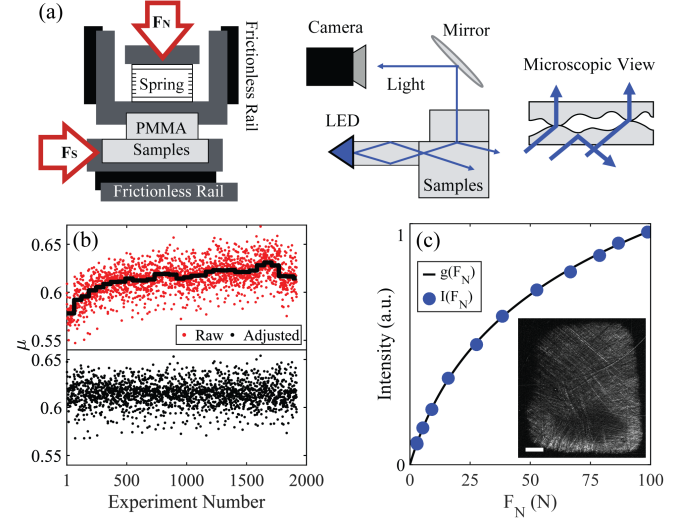

FIG. 1. Experimental setup (a) Schematic of the the biaxial compression/translation stage (top) with integrated optical measurement apparatus (bottom) (b) μ_S vs experiment number for a typical PMMA-PMMA interface before (top) and after (bottom) trend removal described in text. (c) $I(F_N)$ (blue circles) and $g(F_N)$ (black line) vs F_N for a typical loading cycle. Inset: A typical snapshot of an interface illuminated with TIR at $F_N = 100$ N after background subtraction. Scale bar is 1 mm.

response considering that a nonmonotonic evolution occurs while all loading parameters including F_N are held constant. At any two time points in which A_R has the same value before and after T_{min}^A, the load (F_2), and all other macroscopic conditions are identical; however, the system's evolution at these two points is opposite in sign. Thus, the non-monotonic behavior clearly indicates that the state of the system cannot be described by a single variable, and additional degrees of freedom storing a memory of the system's history must exist.

The non-monotonic evolution of A_R for $t > T_W$ follows the sum of two logarithms

$$\Delta A_R(t) = \beta_\Delta \log(t - T_W) + (\beta_2 - \beta_\Delta)\log(t) \qquad (2)$$

with $\beta_\Delta < 0$, and $T_{min}^A \equiv -\beta_\Delta T_W/\beta_2 - T_W$, as shown in Fig. 2(b). This functional form is consistent with the Amir-Oreg-Imry (AOI) model [32, 33], recently proposed as a universal model for aging in disordered systems [20]. In this framework, the relaxation dynamics of glassy systems are facilitated by a spectrum of uncoupled, exponentially relaxing modes, whose density is inversely proportional to their relaxation time scale. These modes may arise from a wide variety of physical processes [34] and in our system may represent modes of plastic creep or adhesive bonding, or any analogous thermally activated process with a distribution of energy barriers that is broad with respect to $k_B T$. All modes relax to an equilibrium that is set by a control parameter, which for the frictional case is F_N. For a two-step protocol, the equi-
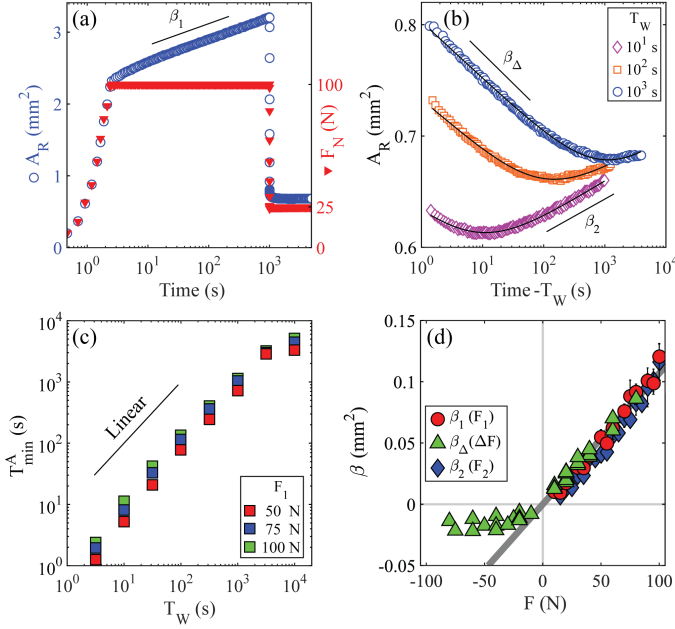
FIG. 2. Glassy dynamics in the real area of contact (a) A_R and F_N vs time for a typical two-step protocol with $F_1 = 100$ N, $T_W = 1000$ s, $F_2 = 25$ N. (b) Evolution of A_R as a function of time shifted by T_W following a step-down in force with $F_1 = 100$ N and $F_2 = 25$ N. Fits (black) use Eq. (2). (c) T_{min}^A as a function of T_W. $F_2 = 25$ N. (d) $\{\beta_1, \beta_\Delta, \beta_2\}$ as a function of $\{F_1, F_\Delta, F_2\}$ respectively. Gray line is a linear fit to $\beta_1(F_1)$ and $\beta_2(F_2)$. Note the deviation of de-aging rate (β_Δ, $F < 0$) from the linear trend.

librium point may change before all modes have fully relaxed; thus, in such a case, non-monotonic evolution may result from fast and slow modes moving in opposite directions. AOI predicts that the evolution of A_R will depend linearly on the parameters in the loading protocol, namely that

$$\frac{T_{min}^A}{T_W} = const \qquad \frac{\beta_1}{F_1} = \frac{\beta_\Delta}{\Delta F} = \frac{\beta_2}{F_2} = const \qquad (3)$$

with $\Delta F \equiv F_2 - F_1$. These predictions, including the form of Eq. (2), also apply to a two-step protocol in which $F_1 < F_2$, albeit with $\beta_\Delta > 0$. Experimentally, we indeed find a linear dependence between T_{min}^A and T_W over several orders of magnitude, as shown in Fig. 2(c). Such a proportionality is a hallmark of real aging and memory [20]. We also find that a step-up protocol ($F_1 < F_2$) yields the same double logarithm evolution (Eq. 2) as the step-down protocol ($F_2 < F_1$), and the logarithmic slopes in both protocols are consistent with Eq. (3), with the notable exception of de-aging, as shown in Fig. 2(d). We return to this later to discuss a possible resolution to this discrepancy, via a modification of AOI that accounts for the instantaneous detachment of microcontacts that results from a drop in F_N.

The non-monotonic effects described above indicate that interfacial memory influences the evolution of the
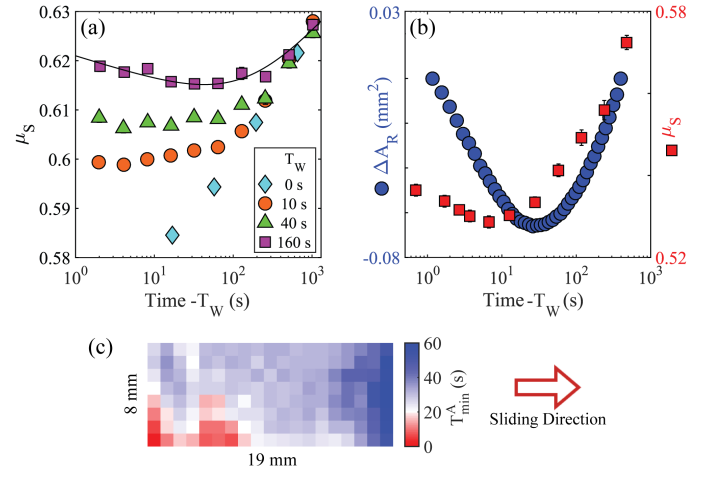
real area of contact. The correspondence between the real area of contact and the static coefficient of friction has been well established [13, 17, 23, 25, 29, 31, 35–37]. However, for aging, the vast majority of these tests relied on a single-step protocol, which shows only continuous logarithmic strengthening, captured well by the Rate and State theory. The non-monotonic relaxation we observe in A_R cannot be captured by any single degree of freedom model, including Rate and State; thus, it is important to test if μ_S also exhibits memory.

Every measurement of μ_S necessitates slip which resets the interface and the experiment. Therefore, while the full evolution of A_R can be continuously measured in a single experiment, the nonmonotonic behavior of the frictional response cannot be verified in a single run, and measuring $\mu_S(t)$ requires numerous repetitions of any single protocol. Comparing $\mu_S(t)$, as shown in Fig. 3(a), to $A_R(t)$ reveals that the two physical quantities exhibit a qualitatively similar memory effect, including non-monotonicity and the increase of T_{min}^μ with T_W. This indicates that a frictional interface is glassy, and can exhibit a real, Kovacs-like memory effect [20]. Following a two-step protocol, $\mu_S(t)$ and $A_R(t)$ both evolve non-monotonically, yet they do not evolve synchronously; strikingly, here $T_{min}^A \neq T_{min}^\mu$. In fact, concurrent measurements of the two quantities show that for an extended period, $\mu_S(t)$ increases whereas $A_R(t)$ continues to decrease, as evidenced by the time period of 8 to 32 seconds in Fig. 3(b). This result points to a simultaneous departure from the Bowden and Tabor framework, as well as from Rate and State Friction.

The discrepancy between $\mu_S(t)$ and $A_R(t)$ emerges

FIG. 3. Memory in static friction (a) μ_S vs time for $F_1 = 90$ N, $F_2 = 25$ N. Line is a guide for the eye to highlight nonmonotonicity. (b) Evolution of A_R and μ_S as a function of time shifted by T_W following a step-down in force with $F_1 = 90$ N, $T_W = 60$ s, $F_2 = 40$ N. (c) Local T_{min}^A for the experiment shown in (b). Notice that local T_{min}^A corresponds to T_{min}^μ, ~ 8s, only over a portion of the interface.

from the complex nature of the spatially extended, 2D interface. Even for carefully prepared surfaces, loading is never perfectly homogenous [25]. As a result, the interface displays a plethora of local responses to a two-step protocol, and T_{min}^A can vary significantly across the interface, as shown in Fig. 3(c). In only a few regions does $A_R(t, x, y)$ shrink and grow in concert with $\mu_S(t)$; less than 15% of the interface has a local T_{min}^A value closer to T_{min}^μ than to global T_{min}^A. This indicates that $A_R(t) = \iint A_R(t, x, y)dxdy$ does not fully represent the state of the interface.

We have shown that both $A_R(t)$ and $\mu_S(t)$ display glassy memory and non-monotonic evolution in time. This behavior cannot be reconciled with a single degree of freedom model like Rate and State Friction, but instead requires a larger spectrum of relaxation modes, such as AOI. Furthermore, we observe $A_R(t)$ and $\mu_S(t)$ evolving asynchronously, and find a dramatic variation in the evolution of $A_R(t, x, y)$ across the interface due to heterogeneity. This variation may explain the inconsistency. It is well accepted that extended bodies with many contact points do not begin sliding uniformly; rather sliding is nucleated within a small region before rapidly propagating outward in a coherent fracture front [25, 29, 31, 36]. In our system, we expect nucleation to occur near the trailing edge of the top sample, as previously reported for identical loading geometries [28, 29, 38]. Therefore, we expect the evolution of μ_S to be dominated by the evolution of $A_R(x, y)$ in that region. Indeed, near the trailing edge, the local values of T_{min}^A and T_{min}^μ match quite well, as shown by comparing Fig. 2(b) and Fig. 3(c).

Taking into account another heterogeneity of the interface may also suggest a resolution to the anomalously weak de-aging rate in the global $A_R(t)$, following the step-down protocol. As previously noted by Greenwood and Williamson [15], when F_N is reduced, the separation between the two surfaces increases, and many microcontacts instantly detach [14, 17]. Any memory stored in a detached microcontact cannot influence the future evolution of A_R. This suggests a generalization of AOI in which each individual mode, i, can engage and disengage at a cutoff height, h_i, uncorrelated with its time constant, λ_i. As a result, instead of a single global equilibrium F_N, each mode's equilibrium is a function $f(h_i - H)$, where $H(F_N)$ is a global parameter. An appealing interpretation of this model considers an ensemble of springs with spring function $f(h_i - H) = k(h_i - H)^\alpha$ for $h_i \geq H$, and 0 for $h_i < H$, compressed from above by a rigid, flat plane under force F_N, as shown in Fig. 4(a). We follow Greenwood and Williamson [15] and assume a normal or an exponential distribution of surface heights, h_i's. Detachment is introduced by stipulating that modes with $h_i < H$ are disregarded. Including detachment has no effect on asymptotic aging (β_1 and β_2), or on positive transient aging (β_Δ for $\Delta F > 0$), but it dramatically re-
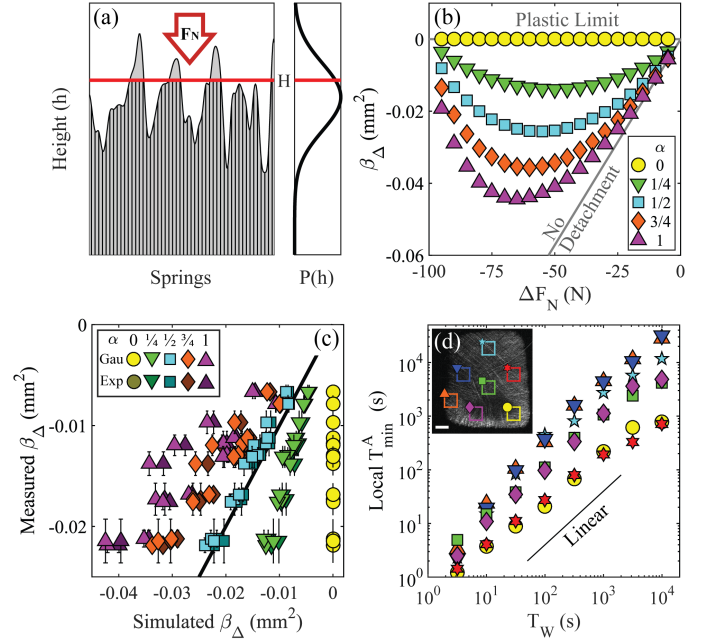

FIG. 4. A phenomenological model for aging of a frictional interface (a) Graphical representation of the ensemble of spring-like modes which compose the interface in the model. A rigid line at global height $H(F_N)$ compresses all springs in contact. Probability of a spring height $P(h)$ is shown on the right. (b) Simulated β_Δ vs ΔF for $F_1 = 100$ N and a Gaussian distribution of heights, $P(h)$. (c) Measured β_Δ vs simulated β_Δ for five values of α. A perfect correspondence would lie on the black, $x = y$ line. Darker and brighter shades correspond to exponential and Gaussian distributions of $P(h)$ respectively. (d) Local T_{min}^A vs T_W for $F_1 = 100$ N, $F_2 = 25$ N. The seven locations are indicated in the inset with corresponding colors. Scale bar is 1 mm.

duces the rate of de-aging (β_Δ for $\Delta F < 0$). We find results are insensitive to the probability distribution of spring heights, $P(h)$, provided they are sufficiently broad [16]. We fit the spring constant, k, to match asymptotic aging data, β_1 and β_2, leaving a single free parameter in the model, α.

The modes can be interpreted as elements of real contact area, in which case $\alpha = 0$ generates the fully plastic, Bowden and Tabor picture [13] where all area in contact carries a set pressure (the yield stress) regardless of normal force. Thus, for $\alpha = 0$ de-aging is completely eliminated, as shown in Fig. 4(b). Correspondingly, $\alpha = 1$ describes an ensemble of Hookean springs whose intitial deformation corresponds to fully elastic interfacial models [14, 15]. The experimental data matches quite well with $\alpha = 1/2$, falling exactly between the fully plastic, $\alpha = 0$ and the fully elastic $\alpha = 1$ limits, as shown in Fig. 4(c). One implication of this model is that rich, non-monotonic aging behavior and the memory effect are not only global properties, but should persist in small subsections of the interface. Indeed, logarithmic aging, de-

aging, and the (quasi) linear scaling of T^A_{min} with T_W are also present locally, as shown in Fig. 4(d). It is natural to wonder onto what small scale the kovacs-like memory effect will persist and whether it could be observed even on a single asperity level.

---

[1] J. H. Dieterich, J. Geophys. Res. **77**, 3690 (1972).
[2] F. Heslot, T. Baumberger, B. Perrin, B. Caroli, and C. Caroli, Phys. Rev. E **49**, 4973 (1994).
[3] T. Baumberger and C. Caroli, Adv. Phys. **55**, 279 (2006).
[4] P. Berthoud, T. Baumberger, C. G'sell, and J. M. Hiver, Phys. Rev. B **59** (1999).
[5] L. Bocquet, E. Charlaix, S. Ciliberto, and J. Crassous, Nature **396**, 735 (1998).
[6] A. D. Corwin and M. P. de Boer, Phys. Rev. B **81**, 174109 (2010).
[7] C. H. Scholz, Nature **391**, 37 (1998).
[8] J. R. Rice, Pure Appl. Geophys. **121**, 443 (1983).
[9] C. Marone, Annu. Rev. Earth Planet. Sci. **26**, 643 (1998).
[10] J. H. Dieterich, J. Geophys. Res. **84**, 2161 (1979).
[11] J. R. Rice and A. Ruina, J. Appl. Mech. **50**, 343 (1983).
[12] A. Ruina, J. Geophys. Res. **88**, 10359 (1983).
[13] F. P. Bowden and D. Tabor, *The Friction and Lubrication of Solids* (Clarendon Press Oxford, 1950).
[14] J. F. Archard, Proc. R. Soc. A , 1 (1957).
[15] J. A. Greenwood and J. B. P. Williamson, Proc. R. Soc. A **295**, 300 (1966).
[16] B. Persson, J. Chem. Phys. (2001).
[17] J. H. Dieterich and B. D. Kilgore, US Geological Survey **143**, 283 (1994).
[18] Q. Li, T. E. Tullis, D. Goldsby, and R. W. Carpick, Nature **480**, 233 (2011).
[19] Y. Liu and I. Szlufarska, Phys. Rev. Lett. **109**, 19 (2012).
[20] Y. Lahini, O. Gottesman, A. Amir, and S. M. Rubinstein, Phys. Rev. Lett. **118**, 394 (2017).
[21] A. J. Kovacs, Adv. Polym. Sci. **3** (1969).
[22] C. Josserand, A. V. Tkachenko, D. M. Mueth, and H. M. Jaeger, Phys. Rev. Lett. **85**, 3632 (2000).
[23] S. M. Rubinstein, G. Cohen, and J. Fineberg, Phys. Rev. Lett. **96**, 256103 (2006).
[24] "See supplementary material for detailed surface analysis,".
[25] S. M. Rubinstein, G. Cohen, and J. Fineberg, Phys. Rev. Lett. (2007).
[26] "Pre-stress protocol procedures are detailed in the supplementary material.".
[27] O. Ben-David and J. Fineberg, Phys. Rev. Lett. (2011).
[28] T. Yamaguchi, Y. Sawae, and S. M. Rubinstein, Ext. Mech. Lett. **9**, 331 (2016).
[29] S. M. Rubinstein, G. Cohen, and J. Fineberg, Nature (2004).
[30] A. I. Bennett, K. L. Harris, K. D. Schulze, J. M. Urueña, A. J. McGhee, A. A. Pitenis, M. H. Müser, T. E. Angelini, and W. G. Sawyer, Tribology Letters , 1 (2017).
[31] S. M. Rubinstein, M. Shay, and G. Cohen, Int. J. Fracture (2006).
[32] A. Amir, Y. Oreg, and Y. Imry, Phys. Rev. B **77**, 689 (2008).
[33] A. Amir, Y. Oreg, and Y. Imry, Phys. Rev. Lett. **103**, 126403 (2009).
[34] A. Amir, Y. Oreg, and Y. Imry, PNAS **109**, 1850 (2012).
[35] O. Ben-David, S. M. Rubinstein, and J. Fineberg, Nature **463**, 76 (2010).
[36] I. Svetlizky and J. Fineberg, Nature **509**, 205 (2014).
[37] S. M. Rubinstein, G. Cohen, and J. Fineberg, J. Phys. D. (2009).
[38] T. Baumberger, C. Caroli, and O. Ronsin, Eur. Phys. J. E **11**, 85 (2003).